Veröffentlichung

Im Rahmen des SFB 880. www.sfb880.tu-braunschweig.de

Autoren

Mößner, Michael;Radespiel, Rolf

Titel

Numerical Simulations of Turbulent Flow over Porous Media

Publisher o. Konferenz

43rd AIAA Fluid Dynamics Conference and Exhibit, San Diego, California, 2013

Jahr

2013

Internet-Link (Doi-Nr.)

Numerical Simulations of Turbulent Flow over Porous Media

M. Mößner * and R. Radespiel †

Technische Universität Braunschweig, Braunschweig, 38108, Germany

A strategy to extending RANS solvers for simulating compressible and turbulent flow into and through porous media is presented. Therefor Darcy and Forchheimer term are appended to the Navier-Stokes equations. Beside of that the effect of porous terms onto the turbulence equations are considered. The interface region between porous and nonporous flow is modelled by an isentropic flow change and corrected by a stress jump condition. The implementation into the flow solver is demonstrated and verified with reference cases. Finally, solutions for a turbulent channel partially filled with cubes are compared with DNS computations.

Nomenclature

A_{fs}	Surface area of porous structure
c_ε	Modelling constant for correlations in dissipation equation
c_F	Forchheimer coefficient
c_t	Modelling constant for velocity fluctuation triple correlations
d	Distance inside porous structure
D_{ij}	Diffusion term in Reynolds stress transport equations
D_ε	Diffusion term in turbulent dissipation equation
e	Internal energy
h	Enthalpy
H	Channel height
k_d	Thermal diffusion
$\vec{n}$	Normal vector
n_i	i-component of normal vector
p	Pressure
P_{ij}	Production term in Reynolds stress transport equations
P_ε	Production terms in turbulent dissipation equation
$\mathcal{P}$	Porous source terms for Reynolds stress transport equations
Re	Reynolds number
t	Time
T	Integration time interval
T_ε	Turbulent transport term in turbulent dissipation equation
u_τ	Shear stress velocity
U_b	Bulk velocity $\rightarrow$ mean velocity inside channel section
v_i	Velocity in direction i
V	Volume
x_i	Coordinate in direction i
Y	Dissipation term in turbulent dissipation equation
z	Coordinate normal to wall or nonporous–porous interface area

*Research Scientist, Institute of Fluid Mechanics, Technische Universität Braunschweig, Hermann-Blenk-Str. 37, 38108 Braunschweig, m.moessner@tu-bs.de, Phone: +49-531-391-94262

†Professor, Institute of Fluid Mechanics, Technische Universität Braunschweig, Hermann-Blenk-Str. 37, 38108 Braunschweig, r.radespiel@tu-bs.de, Phone: +49-531-391-94250, AIAA Senior Member

Greek letters

β	Stress jump coefficient
ε	Dissipation of turbulence
ϵ	Perputation variable
γ	Isentropic exponent
κ	Permeability
μ	Dynamic viscocity
ν	Kinematic viscosity
ϕ	Porosity
Φ	Redistribution term in Reynolds stress transport equations
Φ_ε	Pressure transport term in turbulent dissipation equation
ρ	Density
τ_{ij}	Element i, j of tensor of viscous stresses

Subscript

f	Fluid phase
p	Porous phase
b	Bulk $\rightarrow$ average value over channel section

Averaging

$\overline{\varphi}$	Time average of arbitrary variable φ
$\widetilde{\varphi}$	Density weighted time average of arbitrary variable φ
$\langle\varphi\rangle$	Volume average of arbitrary variable φ
$\langle\varphi\rangle_\mathcal{F}$	Density weighted volume average of arbitrary variable φ
$\varphi^\diamond$	φ-fluctuation value of density weighted volume averaging
φ'	φ-fluctuation value of density weighted time averaging

I. Introduction

The need for drastic noise reductions in commercial aircraft leads to new approaches to minimize the airframe noise sources. One of these concepts is the usage of porous material.[1] Depending on the permeability of the porous material the flow will be influenced which leads to modified aerodynamic properties as well. This is why flow solvers have to be provided with new capabilities to simulate flow over and through porous material.

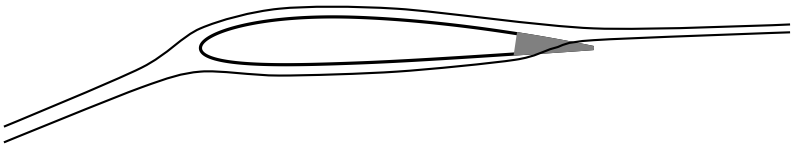

Figure 1. Airfoil with porous trailing edge. The streamlines are significantly influenced and aerodynamic properties are altered.

Several factors are important during the derivation of the numerical approach:

- Turbulence has to be modelled as the Reynolds number of airplanes is high,
- The flow is compressible – a consequence of high Mach numbers
- The porous structure is very fine – the flow inside the porous structure cannot be resolved.

The following sections will show how to comply with these requirements and integrate the resulting equations and models into a flow solver.

II. Theoretical Background

As starting point for the theoretical derivations serve the Navier-Stokes equations:

$$\frac{\partial \rho}{\partial t} + \frac{\partial \rho v_k}{\partial x_k} = 0 \tag{1a}$$

$$\frac{\partial \rho v_i}{\partial t} + \frac{\partial \rho v_i v_k}{\partial x_k} + \frac{\partial p}{\partial x_i} - \frac{\partial \tau_{ik}}{\partial x_k} = 0 \tag{1b}$$

$$\frac{\partial \rho e}{\partial t} + \frac{\partial \frac{1}{2}\rho v_j v_j}{\partial t} + \frac{\partial \rho h v_k}{\partial x_k} + \frac{\partial \frac{1}{2}\rho v_j v_j v_k}{\partial x_k} - \frac{\partial v_j \tau_{jk}}{\partial x_k} - \frac{\partial k_{d,k}}{\partial x_k} = 0 \tag{1c}$$

where t is the time, x_i are the coordinates, ρ is the density, v_i are the velocity components, p is the pressure, τ is the tensor of viscous stresses, e is the internal energy, h is the enthalpy and k_d the thermal diffusion. It is assumed that these equations fully describe the fluid flow inside and outside of a porous medium. Due to the very small pores in many fluid dynamic applications (like the flow past an airplane with porous trailing edges) the flow inside the porous structure cannot be resolved. Also it is not possible to resolve the turbulent structure at high Reynolds numbers. This lack of computational ressources often goes along with the mere interest in the averaged flow properties only.

A. Volume Averaging of the Navier-Stokes Equations

One way to only consider the mean flow and not to resolve the flow inside the porous structure is volume averaging over the fluid state inside the porous material and taking into account the porosity effects by applying additional drag (see figure 2). Spatial averaging can be written as

$$\langle \varphi \rangle = \frac{1}{V_f} \int_{V_f} \varphi \, \mathrm{d}V \tag{2}$$

with V_f being the fluid volume inside the porous structure and φ as arbitrary variable to be averaged. For compressible fluids density weighted averaging keeps the equations simple. It is defined as

$$\langle \varphi \rangle_{\mathcal{F}} = \frac{1}{V_f \langle \rho \rangle} \int_{V_f} \rho \varphi \, \mathrm{d}V = \frac{\langle \rho \varphi \rangle}{\langle \rho \rangle} \quad . \tag{3}$$

When the Navier-Stokes equations are volume averaged additional relations are needed for the derivatives. This is because not the average of the derivative is needed but rather the derivative of an averaged state variable. Bear[2] shows these relations to be

$$\left\langle \frac{\partial \varphi}{\partial t} \right\rangle = \frac{\partial \langle \varphi \rangle}{\partial t} - \frac{1}{V_f} \int_{A_{fs}} \varphi \cdot \vec{v}^T \cdot \vec{n} \, \mathrm{d}A \quad , \quad \langle \nabla \varphi \rangle = \nabla \langle \varphi \rangle + \frac{1}{V_f} \int_{A_{fs}} \varphi \cdot \vec{n} \, \mathrm{d}A \tag{4}$$

where $\vec{n}$ is the normal vector with its direction perpendicular to the pore surfaces A_{fs}.

Additionally, when the Navier-Stokes equations are averaged, the deviations from the mean values will appear. Inhere, for volume averaging the deviation from the density weighed volume average is marked with a diamond:

$$\varphi = \langle \varphi \rangle_{\mathcal{F}} + \varphi^{\diamond} \tag{5}$$

Note that the averaging volume should be large enough that the expressions

$$\langle\langle \varphi \rangle_{\mathcal{F}} \rangle_{\mathcal{F}} = \langle \varphi \rangle_{\mathcal{F}} \quad \text{and} \quad \langle \varphi^{\diamond} \rangle_{\mathcal{F}} = 0$$

are valid.

Using the presented relations the Navier-Stokes equations (1) are averaged in space. After applying some

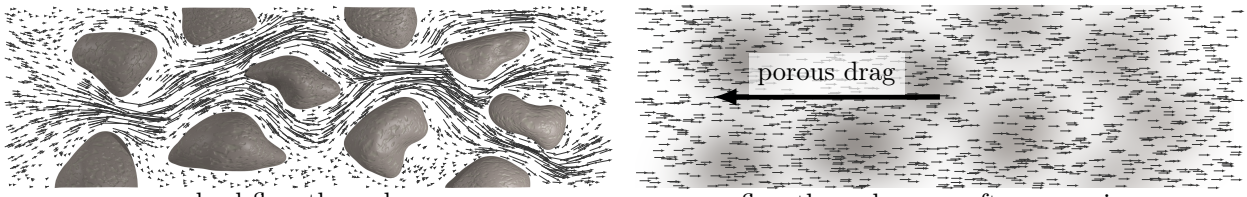

Figure 2. Principle of volume averaging of flow inside a porous structure

common simplifications they result in

$$\frac{\partial\langle\rho\rangle}{\partial t} + \frac{\partial\langle\rho\rangle\langle v_k\rangle_{\mathcal{F}}}{\partial x_k} = 0 \quad (6a)$$

$$\frac{\partial\langle\rho\rangle\langle v_i\rangle_{\mathcal{F}}}{\partial t} + \frac{\partial\langle\rho\rangle\langle v_i\rangle_{\mathcal{F}}\langle v_k\rangle_{\mathcal{F}}}{\partial x_k} + \frac{\partial\langle p\rangle}{\partial x_i} - \frac{\partial\langle\tau_{ik}\rangle}{\partial x_k} + \frac{1}{V_f}\int\limits_{A_{fs}} p\cdot n_i - \tau_{ik}n_k \,\mathrm{d}A = 0 \quad (6b)$$

$$\frac{\partial\langle\rho\rangle\langle e\rangle_{\mathcal{F}}}{\partial t} + \frac{\partial\frac{1}{2}\langle\rho\rangle\langle v_j\rangle_{\mathcal{F}}\langle v_j\rangle_{\mathcal{F}}}{\partial t} + \frac{\partial\langle\rho\rangle\langle h\rangle_{\mathcal{F}}\langle v_k\rangle_{\mathcal{F}}}{\partial x_k} + \frac{\partial\frac{1}{2}\langle\rho\rangle\langle v_j\rangle_{\mathcal{F}}\langle v_j\rangle_{\mathcal{F}}\langle v_k\rangle_{\mathcal{F}}}{\partial x_k} - \frac{\partial\langle v_j\rangle_{\mathcal{F}}\langle\tau_{jk}\rangle}{\partial x_k} - \frac{\partial\langle k_{d,k}\rangle}{\partial x_k} = 0 \quad . (6c)$$

The basic simplification in these equations is that correlations between deviations are neglected. For correlations between two velocity fluctuations this is discussed and examined by Breugem.[3] This assumption is also applied on other correlations in this derivation. Further assumptions are that the velocity is zero at the pore surfaces and that there is no heat transfer between fluid and the porous structure. All these assumptions help to keep equations (6) similar to the original Navier-Stokes equations (1), the surface integral in the momentum equation (6b) being the only difference. This surface integral describes the additional drag inside the porous medium. Typically, it is modelled with Darcy's law which can be extended by a quadratic term called Forchheimer term (see[4] or[5]):

$$\frac{1}{V_f}\int\limits_{A_{fs}} p\cdot n_i - \tau_{ik}n_k \,\mathrm{d}A = \underbrace{\phi\frac{\mu}{\kappa}\langle v_i\rangle_{\mathcal{F}}}_{\text{Darcy}} + \underbrace{\langle\rho\rangle\frac{c_F}{\sqrt{\kappa}}\sqrt{\langle v_k\rangle_{\mathcal{F}}\langle v_k\rangle_{\mathcal{F}}}\langle v_i\rangle_{\mathcal{F}}}_{\text{Forchheimer}} \quad (7)$$

with the dynamic viscosity μ, the porosity ϕ, the permeability κ and the Forchheimer coefficient c_F. The porosity ϕ is defined as the ratio between fluid volume V_f and entire volume V containing also the solid structure of the material. The permeability κ and the Forchheimer coefficient c_F are material specific parameters of the porous medium.

B. Time Averaging of the Volume Averaged Navier-Stokes Equations

Before starting with the discussion of averaging in time note that all variables in equations (6) and (7) are written in their volume averaged form. From now on the volume averaging signs are omitted while keeping in mind that all variables always are volume averaged. This makes the equations more easy to read.

Time averaging of the compressible Navier-Stokes equations is a well known procedure to avoid resolving the turbulent structure and this is described in detail in numerous literature e.g. by Wilcox.[6] The procedure will be addressed only briefly. Only the effects of the porous terms are described in more detail.

The time average and the density weighted time average used are defined as

$$\overline{\varphi} = \frac{1}{T}\int\limits_{T}\varphi\,\mathrm{d}t \quad ; \qquad \widetilde{\varphi} = \frac{1}{\overline{\rho}T}\int\limits_{T}\rho\varphi\,\mathrm{d}t \quad (8)$$

with the time interval T. The density weighted average will also be used together with its fluctuation value which is defined in terms of

$$\varphi = \widetilde{\varphi} + \varphi'$$

where

$$\widetilde{\widetilde{\varphi}} = \widetilde{\varphi} \quad \text{and} \quad \widetilde{\varphi'} = 0 \ .$$

Inserting equation (7) into (6) and averaging in time results in

$$\frac{\partial \overline{\rho}}{\partial t} + \frac{\partial \overline{\rho}\widetilde{v_k}}{\partial x_k} = 0 \tag{9a}$$

$$\frac{\partial \overline{\rho}\widetilde{v_i}}{\partial t} + \frac{\partial \overline{\rho}\widetilde{v_i}\widetilde{v_k}}{\partial x_k} + \frac{\partial \overline{\rho}\widetilde{v_i'v_k'}}{\partial x_k} + \frac{\partial \overline{p}}{\partial x_i} - \frac{\partial \overline{\tau_{ik}}}{\partial x_k} + \underbrace{\phi\frac{\mu}{\kappa}\widetilde{v_i}}_{\text{Darcy}} + \underbrace{\overline{\rho}\frac{c_F}{\sqrt{\kappa}}\widetilde{\sqrt{v_k v_k}v_i}}_{\text{Forchheimer}} = 0 \tag{9b}$$

$$\begin{aligned}&\frac{\partial \overline{\rho}\widetilde{e}}{\partial t} + \frac{\partial \frac{1}{2}\overline{\rho}\widetilde{v_j}\widetilde{v_j}}{\partial t} + \frac{\partial \frac{1}{2}\overline{\rho}\widetilde{v_j'v_j'}}{\partial t} + \frac{\partial \overline{\rho}\widetilde{h}\widetilde{v_k}}{\partial x_k} + \frac{\partial \overline{\rho}\widetilde{h'v_k'}}{\partial x_k} + \frac{\partial \frac{1}{2}\overline{\rho}\widetilde{v_j}\widetilde{v_j}\widetilde{v_k}}{\partial x_k} \\ &+\frac{\partial \frac{1}{2}\overline{\rho}\widetilde{v_k}\widetilde{v_j'v_j'}}{\partial x_k} + \frac{\partial \overline{\rho}\widetilde{v_j}\widetilde{v_j'v_k'}}{\partial x_k} + \frac{\partial \frac{1}{2}\overline{\rho}\widetilde{v_j'v_j'v_k'}}{\partial x_k} - \frac{\partial \widetilde{v_j}\overline{\tau_{jk}}}{\partial x_k} - \frac{\partial \overline{v_j'\tau_{jk}}}{\partial x_k} - \frac{\partial \overline{k_{d,k}}}{\partial x_k} = 0 \ .\end{aligned} \tag{9c}$$

The form of these equations differ from the equations (1) by the Darcy and Forchheimer term and the correlations of fluctuation values. The Darcy and Forchheimer term describe the effect of porosity and the correlations of fluctuation values appear as a consequence of turbulence. The average of the velocities in the Forchheimer term is inconvenient and has to be reformulated in a way that only the average of single velocities remain. This can be achieved by using a Taylor expansion:

$$f(\epsilon = 1) = f(\epsilon = 0) + \left.\frac{\partial f(\epsilon)}{\partial \epsilon}\right|_{\epsilon=0} + \frac{1}{2}\left.\frac{\partial^2 f(\epsilon)}{\partial \epsilon^2}\right|_{\epsilon=0} + \dots$$

where

$$f(\epsilon) = \widetilde{\sqrt{v_k v_k}v_i} \quad \text{with} \quad v_{i/k} = \widetilde{v_{i/k}} + \epsilon \cdot v_{i/k}'$$

with $\epsilon = 0$ being the reference state and $\epsilon = 1$ being the state where the Taylor expansion is evaluated. Using these definitions finally results in a second order approximation of the Forchheimer term:

$$\overline{\rho}\frac{c_F}{\sqrt{\kappa}}\widetilde{\sqrt{v_k v_k}v_i} = \overline{\rho}\frac{c_F}{\sqrt{\kappa}}\left[\sqrt{\widetilde{v_l}\widetilde{v_l}}\cdot\widetilde{v_i} + \frac{1}{2}\frac{\widetilde{v_i}}{\sqrt{\widetilde{v_l}\widetilde{v_l}}}\widetilde{v_j'v_j'} + \frac{\widetilde{v_j}}{\sqrt{\widetilde{v_l}\widetilde{v_l}}}\widetilde{v_i'v_j'} - \frac{1}{2}\frac{\widetilde{v_i}\widetilde{v_j}\widetilde{v_k}}{\sqrt{(\widetilde{v_l}\widetilde{v_l})^3}}\widetilde{v_j'v_k'}\right] \ . \tag{10}$$

C. Modelling of Turbulence

The presence of turbulence leads to correlations between fluctuations. All these correlations which appear in equations (9b) and (9c) have to be specified. For modelling these effects of turbulence a Reynolds stress model is applied for reasons of complex flow behaviours such as streamline curvature and flow rotation. The basic derivations of Reynolds stress and dissipation transport equations are extensively discussed by Wilcox.[6] Written in a simple form the Reynolds stress equation are

$$\frac{\partial \overline{\rho}\widetilde{v_i'v_j'}}{\partial t} + \frac{\partial \overline{\rho}\widetilde{v_k}\widetilde{v_i'v_j'}}{\partial x_k} = P_{ij} + \Phi_{ij} + D_{ij} + \varepsilon_{ij} - \overline{v_j'}\frac{\partial \overline{p}}{\partial x_i} - \overline{v_i'}\frac{\partial \overline{p}}{\partial x_j} \tag{11}$$

without considering porosity effects. The terms are named according to literature: P is the production term, Φ is the redistribution term, D is the diffusion term and ε is the dissipation term. The dissipation equation can be written as

$$\frac{\partial \overline{\rho}\varepsilon}{\partial t} + \frac{\partial \overline{\rho}\widetilde{v_k}\varepsilon}{\partial x_k} = P_\varepsilon^1 + P_\varepsilon^2 + P_\varepsilon^3 + P_\varepsilon^4 + T_\varepsilon + \Phi_\varepsilon + D_\varepsilon - Y \tag{12}$$

where the terms P_ε are production terms, T_ε is the turbulent transport term, Φ_ε is the pressure transport term, D_ε is the diffusion term and Y is the dissipation term according to Mansour et al.[7]

In the present paper the terms are modelled according to the *JHh-v2* turbulence model.[8] The remaining unknown correlation terms in the energy equation (9c) are modelled with the gradient diffusion hypothesis and a turbulent Prandtl number.

Now the question arises how the turbulence is influenced inside porous media. This problem can be dealt with by deriving the exact Reynolds stress transport equations starting from the volume averaged

momentum equations (6b). This leads to the additional terms

$$\mathcal{P}_{\mathrm{RS,Darcy}} = -\phi\frac{\mu}{\kappa}\left[\overline{v_i'}\widetilde{v_j} + \overline{v_j'}\widetilde{v_i} + 2\overline{v_i'v_j'}\right] \tag{13a}$$

$$\begin{aligned}\mathcal{P}_{\mathrm{RS,Forch}} = -\frac{c_F}{\sqrt{\kappa}}\overline{\rho}\Bigg[&2\widetilde{v_i'v_j'}\sqrt{\widetilde{v_l}\widetilde{v_l}} + \frac{\widetilde{v_j}\widetilde{v_k}}{\sqrt{\widetilde{v_l}\widetilde{v_l}}}\widetilde{v_i'v_k'} + \frac{\widetilde{v_i}\widetilde{v_k}}{\sqrt{\widetilde{v_l}\widetilde{v_l}}}\widetilde{v_j'v_k'} + 2\frac{\widetilde{v_k}}{\sqrt{\widetilde{v_l}\widetilde{v_l}}}\widetilde{v_i'v_j'v_k'} + \frac{1}{2}\frac{\widetilde{v_j}}{\sqrt{\widetilde{v_l}\widetilde{v_l}}}\widetilde{v_i'v_k'v_k'} \\ &+ \frac{1}{2}\frac{\widetilde{v_i}}{\sqrt{\widetilde{v_l}\widetilde{v_l}}}\widetilde{v_j'v_k'v_k'} - \frac{1}{2}\frac{\widetilde{v_j}\widetilde{v_m}\widetilde{v_k}}{\sqrt{(\widetilde{v_l}\widetilde{v_l})^3}}\widetilde{v_i'v_m'v_k'} - \frac{1}{2}\frac{\widetilde{v_i}\widetilde{v_m}\widetilde{v_k}}{\sqrt{(\widetilde{v_l}\widetilde{v_l})^3}}\widetilde{v_j'v_m'v_k'}\Bigg]\end{aligned} \tag{13b}$$

inside the Reynolds stress equations (11). Doing a similar procedure for the dissipation equation results in

$$\mathcal{P}_{\varepsilon,\mathrm{Darcy}} = -2\phi\frac{\mu}{\kappa}\varepsilon \tag{14a}$$

$$\begin{aligned}\mathcal{P}_{\varepsilon,\mathrm{Forch}} = -\overline{\rho}\frac{c_F}{\sqrt{\kappa}}\Bigg[&2\sqrt{\widetilde{v_l}\widetilde{v_l}}\cdot\varepsilon + \nu\frac{\partial\sqrt{\widetilde{v_l}\widetilde{v_l}}}{\partial x_j}\frac{\partial\widetilde{v_i'v_i'}}{\partial x_j} + 2\nu\frac{\widetilde{v_k}}{\sqrt{\widetilde{v_l}\widetilde{v_l}}}\left[\widetilde{v_k'\frac{\partial v_i'}{\partial x_j}\frac{\partial v_i'}{\partial x_j}} + 2\widetilde{v_i'\frac{\partial v_i'}{\partial x_j}\frac{\partial v_k'}{\partial x_j}} + \widetilde{v_i}\widetilde{\frac{\partial v_i'}{\partial x_j}\frac{\partial v_k'}{\partial x_j}}\right] \\ &+ \nu\frac{\partial}{\partial x_j}\left(\frac{\widetilde{v_k}}{\sqrt{\widetilde{v_l}\widetilde{v_l}}}\right)\left[2\widetilde{v_i'v_k'\frac{\partial v_i'}{\partial x_j}} + \widetilde{v_i'v_i'\frac{\partial v_k'}{\partial x_j}}\right] + \nu\frac{\partial}{\partial x_j}\left(\frac{\widetilde{v_i}\widetilde{v_k}}{\sqrt{\widetilde{v_l}\widetilde{v_l}}}\right)\frac{\partial\widetilde{v_i'v_k'}}{\partial x_j} \\ &- 2\nu\frac{\widetilde{v_i}\widetilde{v_m}\widetilde{v_k}}{\left(\sqrt{\widetilde{v_l}\widetilde{v_l}}\right)^3}\widetilde{v_k'\frac{\partial v_i'}{\partial x_j}\frac{\partial v_m'}{\partial x_j}} - \frac{1}{3}\nu\frac{\partial}{\partial x_j}\left(\frac{\widetilde{v_i}\widetilde{v_m}\widetilde{v_k}}{\left(\sqrt{\widetilde{v_l}\widetilde{v_l}}\right)^3}\right)\frac{\partial\widetilde{v_i'v_m'v_k'}}{\partial x_j}\Bigg]\end{aligned} \tag{14b}$$

as additional terms inside equation (12) where $\nu = \frac{\mu}{\overline{\rho}}$ is the kinematic viscosity. Corresponding to the porosity terms in the momentum equation the Forchheimer terms are second order Taylor expansions to avoid averaging over the entire square roots.

The triple correlations in equation (13b) are modelled by the model of Hanjalic and Launder[9]

$$\widetilde{v_i'v_j'v_k'} = c_t\frac{k}{\varepsilon}\left[\widetilde{v_i'v_l'}\frac{\partial\widetilde{v_j'v_k'}}{\partial x_l} + \widetilde{v_j'v_l'}\frac{\partial\widetilde{v_i'v_k'}}{\partial x_l} + \widetilde{v_k'v_l'}\frac{\partial\widetilde{v_i'v_j'}}{\partial x_l}\right] \tag{15}$$

with a modelling constant c_t and the turbulent energy $k = \widetilde{u_i'u_i'}$. The unknown correlations in equation (14b) are modelled according to Getachew, Minkowycz and Lage.[5] Using the gradient diffusion hypothesis and the assumption of local isotropy inside the porous regions leads to following models:

$$\widetilde{v_k'\frac{\partial v_i'}{\partial x_j}\frac{\partial v_i'}{\partial x_j}} + 2\widetilde{v_i'\frac{\partial v_i'}{\partial x_j}\frac{\partial v_k'}{\partial x_j}} = -\frac{c_\varepsilon}{\nu}\frac{k}{\varepsilon}\widetilde{v_k'v_i'}\frac{\partial\varepsilon}{\partial x_i} \quad ; \quad \widetilde{v_i}\widetilde{\frac{\partial v_i'}{\partial x_j}\frac{\partial v_k'}{\partial x_j}} = \frac{1}{3\nu}\widetilde{v_k}\varepsilon \tag{16}$$

with the modelling constant c_ε. The higher order terms are neglected.

D. Modelling of the interface area between the porous and the free flow region

The derivation of the porous Navier-Stokes equations is based on the assumption of constant porosity. This is not valid close to the interface area as is explained in figure 3.

The modelling procedure of the interface region is split into flow normal and the flow tangential to the porous surface. The case of normal flow is modelled by the assumption of an isentropic flow change. This can be expressed by

$$\text{Mass conservation:} \quad \rho_f\cdot v_{n,f} = \phi\cdot\rho_p\cdot v_{n,p} \tag{17a}$$

$$\text{Energy conservation:} \quad \frac{\gamma}{\gamma-1}\frac{p_f}{\rho_f} + \frac{v_f^2}{2} = \frac{\gamma}{\gamma-1}\frac{p_p}{\rho_p} + \frac{v_p^2}{2} \tag{17b}$$

$$\text{Isentropic condition:} \quad \frac{p_f}{\rho_f^\gamma} = \frac{p_p}{\rho_p^\gamma} \tag{17c}$$

$$\text{Turbulence quantities:} \quad \left[\widetilde{v_i'v_j'}\right]_f = \left[\widetilde{v_i'v_j'}\right]_p \quad ; \quad \varepsilon_f = \varepsilon_p \tag{17d}$$

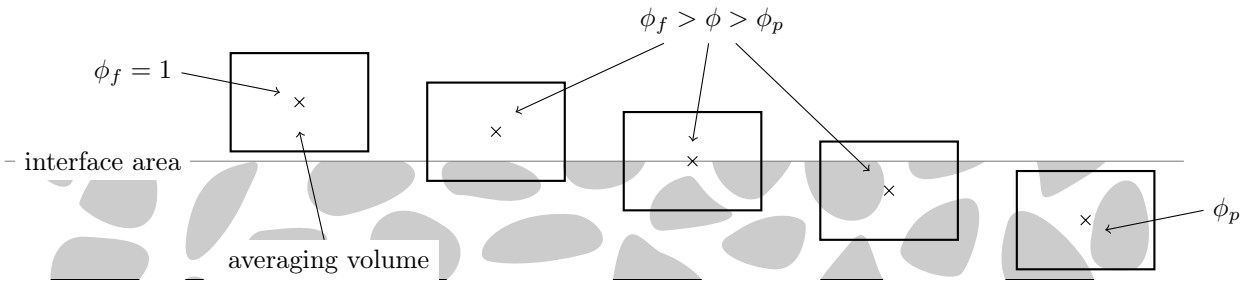

Figure 3. The porosity of an averaging volume close to the interface regions between porous and nonporous flow is not constant.

with γ as isentropic exponent and the velocities v_n normal to the interface area. The subscripts f and p refer to the interface side of nonporous flow and the side of porous flow. Equations (17a)-(17c) are solved using the Newton method.

When the flow velocity is tangential to the nonporous–porous interface the flow over the interface area is defined by diffusion. In principle the interface is set up in a way that diffusion flow always tends to reduce the state variable differences. However, an exception is made for the tangential velocities. Diffusion will urge them to fulfill the relation

$$v_{t,f} = v_{t,p} \cdot \phi \tag{18}$$

where $v_{t,f}$ and $v_{t,p}$ are the velocities tangential to the surface. This relation is borrowed from literature[3] which provides us with DNS data for our validation process. For high porosities it reveals to be a valid assumption. Applying this relation to lower porosities still has to be validated.

There will be shortcomings of these interface modelling approaches especially for flow tangential to the surface of the porous medium. These shortcomings can be accredited to the porous forces which are not accurate close to the interface and have to be corrected. In consequence an additional force is applied tangential to the interface. One way to determine the magnitude of this correction force is the relation

$$\mu \cdot \frac{\partial v_{t,f}}{\partial n} - \mu \cdot \frac{\partial v_{t,p}}{\partial n} = \beta \frac{\mu}{\sqrt{\kappa}} v_{t,f} \tag{19}$$

which is discussed in literature[3,10] and promises good results. In words, the indicator which controls the force is the jump of shear stresses over the nonporous–porous interface area. This jump has to reach the value of $\frac{\mu}{\sqrt{\kappa}} v_{t,f}$ multiplied with a jump coefficient β which has a magnitude of order 1 and depends on the porous structure. The effect of the jump coefficient β on the velocity profile is sketched in figure 4.

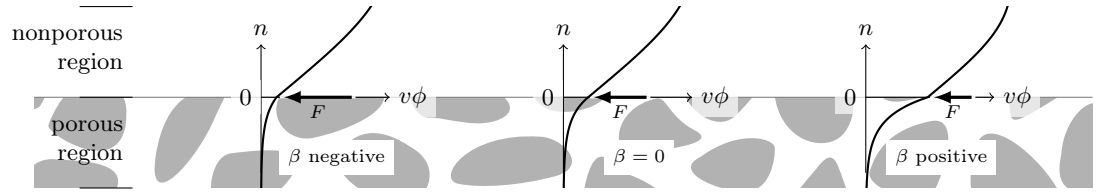

Figure 4. Boundary layer profile for different jump coefficients β.

III. Integration of Porous Wall Capabilities into the Flow Solver TAU

In this section a numerical approach is presented to integrate the introduced equations into a flow solver. This is shown for the flow solver TAU which is developed at the DLR (Deutsches Zentrum für Luft- und Raumfahrt).[11] TAU is an unstructured solver based on the finite volume method.

The integration of porous capabilities can be separated into two tasks as shown in figure 5. First, all porous parts get additional attributes like porosity ϕ, permeability κ and Forchheimer coefficient c_F. These are needed to compute additional source terms according to equation (9b).

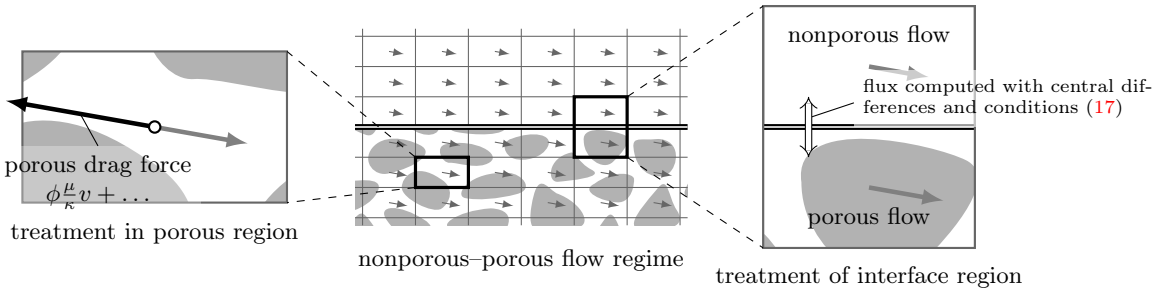

Figure 5. Details of integration of flow through porous media into a finite volume flow solver

The second part of the porous TAU extension are the interface areas between nonporous and porous regions. The flux over these interfaces shall be computed by a central scheme. The central scheme cannot be applied directly because there is a jump in momentum caused by a sudden change of pressure described by the isentropic conditions (17). This problem can be overcome if the cells in the porous region are converted to fictive nonporous region cell using conditions (17). Now the fluxes into the nonporous cell can be computed by a central scheme using the newly created fictive flow inside the porous cell and the real conditions inside the nonporous cell. The described method is also applied inversely by converting the nonporous flow conditions into a fictive porous cell and then computing the flux into the porous cell. Figure 6 visualizes the procedure. The fictive cells are also used to compute the gradients over the porous interface which become important especially for velocity vectors tangential to the interface area.

Finally, the residuals at the interface cells are modified to fulfill the jump condition (19). The additional tangential force needed is determined by an integral type controller. The basic setup is illustrated in figure 7. After each iteration step of the solver the right hand side of equation (19) is compared with its left hand side. The difference is added to the tangential force until equation (19) is fulfilled.

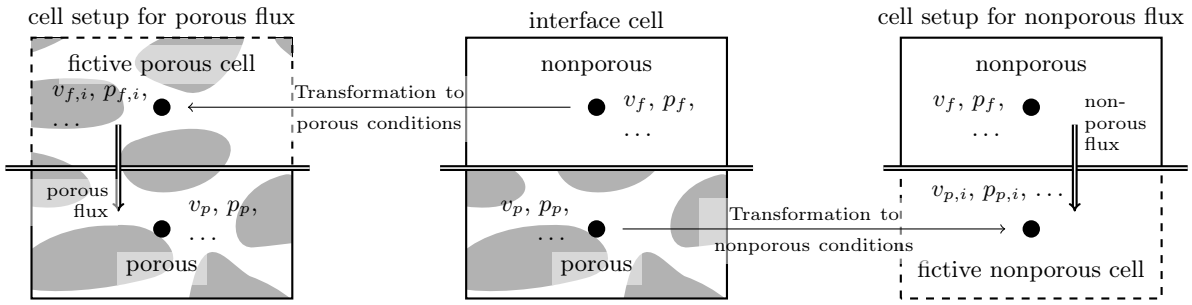

Figure 6. Usage of fictive volume cells to compute fluxes over nonporous–porous interface areas.

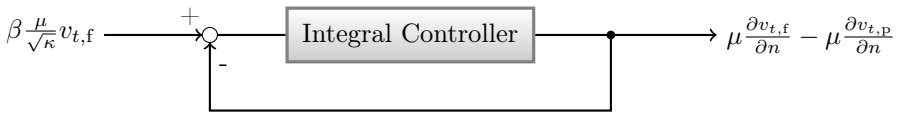

Figure 7. Controlling strategy to adjust the correction force at the porous surface to fulfill the stress jump condition.

IV. Verification Cases

This section will demonstrate verification and validation experiments of the theoretical part of this paper using three generic cases. The valid implementation of Darcy and the isentropic flow change at the porous boundary will be shown with help of a laminar channel flow. The case of laminar flow along a porous boundary is verified with an analytic boundary layer solution over porous media. Finally, a turbulent channel filled

with cubes is compared with DNS computations.

A. Verification of the Darcy term and the Isentropic Flow Change at Porous Surfaces

The verification of the Darcy term is done with help of a channel flow. The first half of the channel is nonporous and the second part is fully porous. The porous interface where the air flows into the porous region is located half of the channel length downstream. Here, the velocity has to increase due to the isentropic flow change described in equations (17). Inside the porous region the pressure will drop steadily in consequence of the drag described by the Darcy term.

The channel geometry is prescribed by using slip-flow boundary conditions. This implies that no boundary layer will develop. The porous region has a permeability of $\kappa = 1 \cdot 10^{-8}\,\mathrm{m}^2$ and the porosity is $\phi = 0.5$. The inflow velocity is $2.8\,\frac{\mathrm{m}}{\mathrm{s}}$ and the viscosity is $1.74 \cdot 10^{-5}\,\frac{\mathrm{kg}}{\mathrm{m\,s}}$.

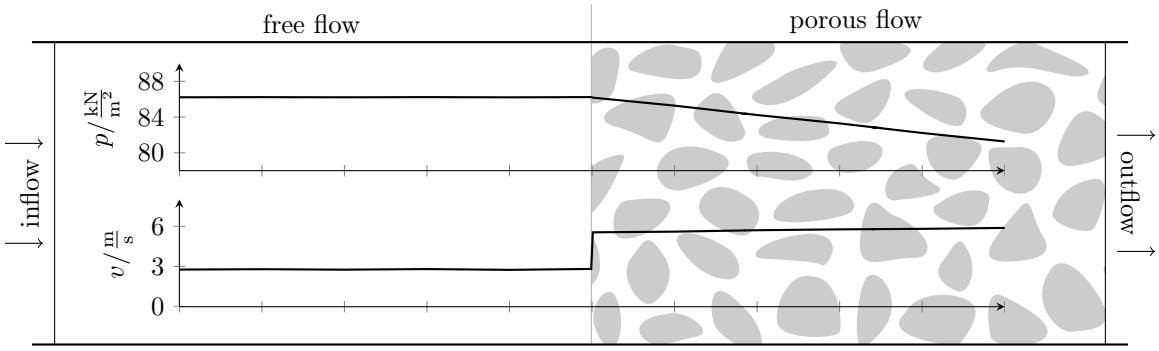

Figure 8. Verification of porous flow in a partly porous channel.

The results computed by the flow solver TAU are shown in figure 8. The correct implementation of the theoretical equations becomes apparent: The flow velocity doubles at the interface due to the porosity of $\phi = 0.5$. This is the result of isentropic flow change applied for incompressible flow. Also, the pressure inside the porous region drops in accordance with the theory of Darcy. This theory defines the pressure gradient $\frac{\partial p}{\partial x}$ by

$$\frac{\partial p}{\partial x} = \phi \frac{\mu}{\kappa} v = 0.5 \cdot \frac{1.74 \cdot 10^{-5}\,\frac{\mathrm{kg}}{\mathrm{m\,s}}}{1 \cdot 10^{-8}\,\mathrm{m}^2} \cdot 5.6\,\frac{\mathrm{m}}{\mathrm{s}} = 4.9\,\frac{\mathrm{kN}}{\mathrm{m}^3} \tag{20}$$

where the numerical solution also gives

$$\frac{\partial p}{\partial x} = \frac{\Delta p}{\Delta x} = \frac{86.2\,\frac{\mathrm{kN}}{\mathrm{m}^2} - 81.3\,\frac{\mathrm{kN}}{\mathrm{m}^2}}{1\,\mathrm{m}} = 4.9\,\frac{\mathrm{kN}}{\mathrm{m}^3}\ .$$

B. Laminar Boundary Layer over a Porous Surface

The second verification case is a laminar boundary layer over a porous surface. Breugem[3] derived an analytic set of equations for porous boundary layers. The equations are based on the Blasius solutions. A superposition of the additional terms takes account for the influence of the porous region.

In the setup the farfield velocity is $v = 66.3\,\frac{\mathrm{m}}{\mathrm{s}}$, the density is $\rho = 0.52\,\frac{\mathrm{kg}}{\mathrm{m}^3}$ and the viscosity is $\mu = 1.74 \cdot 10^{-5}\,\frac{\mathrm{kg}}{\mathrm{m\,s}}$. The porous medium has a permeability of $\kappa = 1 \cdot 10^{-8}\,\mathrm{m}^2$ and a porosity of $\phi = 0.5$. The boundary layer is evaluated $x = 0.5\,\mathrm{m}$ after the start of the porous region.

Figure 9 compares the analytic boundary layer with the solution of the flow solver TAU. The two results are very close to each other and verify the porous implementation for boundary layer flow.

C. Turbulent Channel with Cubes as Porosity

Finally, turbulent flow will be validated inside a partly porous channel. Breugem[4] presented the results of a DNS computation in a channel where the lower half is filled with cubes. See figure 10 for a sketch of the setup. The cubes inside the lower half have a side length of $d_p = 0.05H$ and a spacing between each other of $d_f = 0.05H$ where the H is the nonporous channel height. For the DNS computations the cubes are similarly arranged into the third dimension. The side walls of the channel are set as symmetry planes.

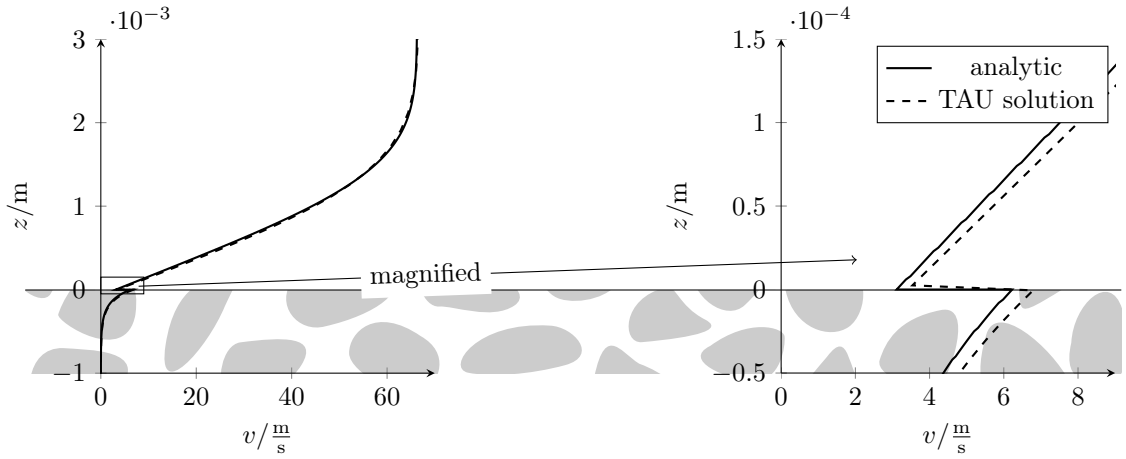

Figure 9. Boundary layer flow over a porous surface. The solution of the modified flow solver TAU is compared with the analytic boundary layer based on the theory of Breugem.[3]

The porosity properties of the grid of cubes are as follows. The porosity is $\phi = 0.875$, the permeability is $\kappa = 3.4 \cdot 10^{-4} H^2$ and the Forchheimer coefficient is $c_F = 0.02$ as referred by Breugem.[4] The jump coefficient is held constant at a value of $\beta = -0.5$. The Reynolds number based on the channel height H and the averaged velocity U_b on the upper half of the channel is $Re_b = 5500$. The Reynolds stress turbulence model *JHh-v2*[8] is used for the volume and time averaged Navier-Stokes equations.

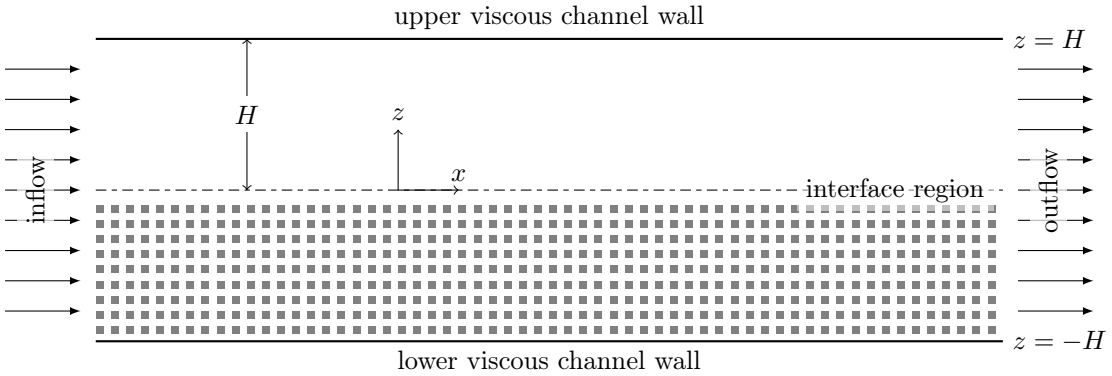

Figure 10. Setup of turbulent channel with cubes in the lower half as porosity as used from Breugem[4] for DNS computations.

In the following the influence of the different turbulence terms inside the porous regions will be shown. Firstly, equations (9) are used together with the standard turbulence equations (11) and (12). The results of the velocity and Reynolds stresses are given in figure 11. These results show that the velocity profile is already rather close to the DNS computations. Also, the Reynolds stresses show only small deviations from the DNS values. The Reynolds stresses $\widetilde{v_x' v_x'}$ inside the porous region obtain a somewhat smaller value due to the lack of turbulence production. As the velocity is very small inside the lower porous region the velocity profile is not affected by this behaviour.

As a second step we investigate how the Darcy term inside the Reynolds stress equations influcences the Reynolds stresses. The Darcy term is given in equations (13a) and (14a) and will damp the Reynolds stresses inside the porous region. In figure 12 one can see the strong effect of the Darcy term onto the Reynolds stresses if compared with the solutions in figure 11. This strong effect is rather unexpected since Breugem[4] compared a pores-resolving DNS with a volume averaging DNS and obtained much better agreement. Further simulations with a systematic variation of porosity and permeability are needed to fully understand the behaviour of our current RANS simulations. Therefor, data reported from Breugem[3] will serve as reference basis.

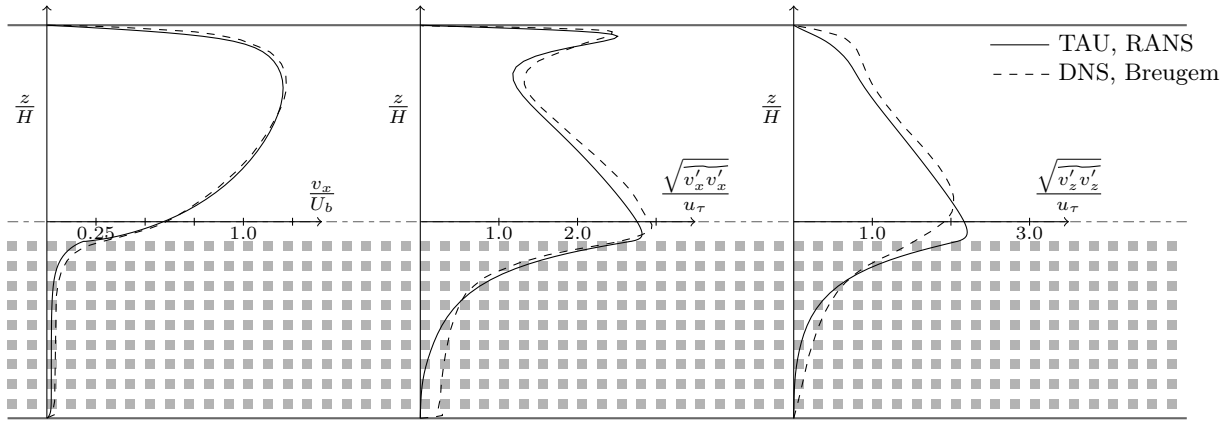

Figure 11. Comparison of VRANS solution with the DNS of Breugem[4] without using the porous terms inside the turbulence equations.

In figure 12 a simulation with only the Forchheimer term switched on is shown. It can be recognized that its effect is similar to the effect of the Darcy term as it damps the the Reynolds stresses significantly inside the porous region. The velocity and Reynolds stress profiles with the total effect of both, Darcy and Forchheimer term is shown in figure 13.

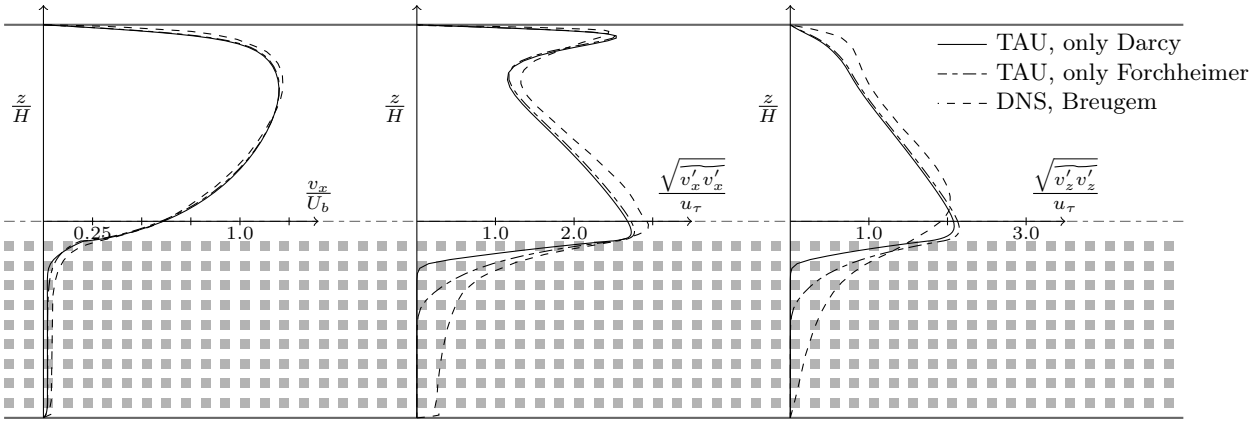

Figure 12. Comparison of VRANS solution with the DNS of Breugem[4] when taken into account the Darcy term or the Forchheimer term respectively inside the turbulence equations.

V. Summary and Conclusion

The arising need for numerical flow simulations in aircraft aerodynamics that include the effects of porous surfaces is the motivation to integrate porous surface media capabilities into the flow solver TAU. To prepare the TAU-code for aeronautical applications several requirements have to be fullfilled: The equations have to model compressible flow at high Mach numbers, advanced turbulence modelling is needed (Reynolds stress models) and the porous models have to be formulated in a way that they can be integrated into a proven flow solver.

The basic procedure to integrate porous capabilities into a flow solver is as follows. The Navier-Stokes equations are extended with porous terms by averaging over a sample of pores. This avoids the need for resolving the porous structure. In our present work, the volume averaging is based on the assumption of constant porosity. In consequence, further modelling has to be accomplished at the interface between porous and nonporous flow. The main modelling principles introduced for that purpose are isentropic flow change for flow perpendicular to the porous surface and a stress jump condition to correct the tangential boundary layer profile. The modelling of turbulence is based on the Reynolds stress model *JHhv2*. The underlying

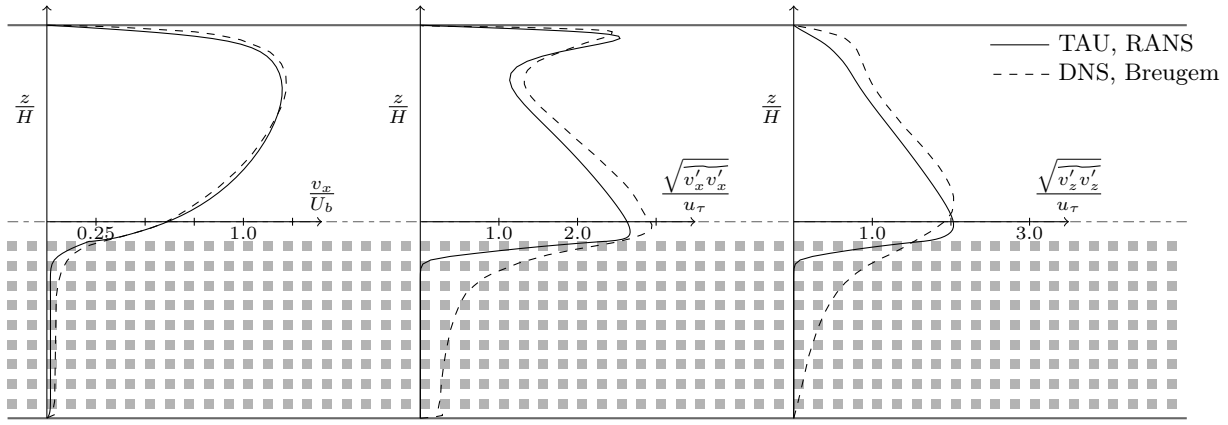

Figure 13. Comparison of VRANS solution with the DNS of Breugem[4] when all porous terms are switched on inside the turbulence equations.

equations are the Reynolds stress transport equations and the dissipation equation. They are extended in our work to be also valid inside porous regions.

The resulting porous modelling equations are integrated into a flow solver. Drag caused by the porous medium is added in form of source terms to the residual of each volume cell. Fictive porous cells and a controlling strategy are introduced to fulfill the interface conditions between porous and nonporous regions. The correct implementation of flow through and over porous media into the flow solver is verified for laminar flow with a porous channel and a boundary layer over a porous surface. The results are in accordance with analytic reference cases.

Validation for turbulent shear flows asks for pores resolving DNS. They are available from the work of Breugem[3] and describe turbulent channel flow with a one-sided porous wall composed of geometrically simple cubes. The setup of Breugem is recalculated with the flow solver. Especially, inside the nonporous regions the results are very similar to the DNS data as shown with the velocity and Reynolds stress profiles. Inside the porous material the the porous terms inside the Reynolds stress equation lead to sharp falloff of the Reynolds stresses which is not obtained in the reference DNS data. More comparisons of RANS and DNS data are needed to investigate this behaviour.

References

[1]Herr, M., "Design Criteria for Low-Noise Trailing-Edges," *13th AIAA/CEAS Aeroacoustics Conference*, DLR, German Aerospace Center, 38108 Braunschweig, 2007.

[2]Bear, J. and Bachmat, Y., *Introduction to modeling of transport phenomena in porous media*, Vol. 4 of *Theory and applications of transport in porous media*, Kluwer Academic Publishers, 1990.

[3]Breugem, W.-P., *The influence of wall permeability on laminar and turbulent flows*, Ph.D. thesis, Technische Universiteit Delft, 1 2005.

[4]Breugem, W. P. and Boersma, B. J., "Direct numerical simulations of turbulent flow over a permeable wall using a direct and a continuum approach," *Physics of Fluids*, Vol. 17, 2005.

[5]Getachew, D., Minkowycz, W. J., and Lage, J. L., "A modified form of the κ-ε model for turbulent flows of an incompressible fluid in porous media," *International Journal of Heat and Mass Transfer*, Vol. 43, 2000, pp. 2909–2915.

[6]Wilcox, D. C., *Turbulence Modeling for CFD*, DCW Industries, 3rd ed., 2006.

[7]Mansour, N. N., J., K., and P., M., "Reynolds-stress and dissipation-rate budgets in a turbulent channel flow," *Journal of Fluid Mechanics*, Vol. 194, 1988, pp. 15–44.

[8]Cécora, R.-D., Eisfeld, B., Probst, A., Crippa, S., and Radespiel, R., "Differential Reynolds Stress Modeling for Aeronautics," Nashville, Tennessee, 1 2012.

[9]Hanjalić, K. and Launder, B. E., "Contribution towards a Reynolds-stress closure for low-Reynolds-number turbulence," *Journal of Fluid Mechanics*, Vol. 74, 1976, pp. 593–610.

[10]de Lemos, M. J. S. and Silva, R. A., "Turbulent flow over a layer of a highly permeable medium simulated with a diffusion-jump model for the interface," *International Journal of Heat and Mass Transfer*, Vol. 49, 2006, pp. 546–556.

[11]Schwamborn, D., Gerhold, T., and Heinrich, R., "The DLR TAU-Code: Recent Applications in Research and Industry," *ECCOMAS CFD 06*, edited by P. Wesseling, E. Oñate, and J. Périaux, TU Delft, The Netherlands, 9 2006.